Mechanical Interlocking Enhances the Electrocatalytic Oxygen Reduction Activity and Selectivity of Molecular Copper Complexes

Xiaoyong Mo,[1,6] Yulin Deng,[1,6] Samuel Kin-Man Lai,[1] Xutao Gao,[1] Hung-Ling Yu,[3,4] Kam-Hung Low,[1] Heng-Liang Wu,[3,4] Ho Yu Au-Yeung,[1,5,*] Edmund C. M. Tse [1,2,*]

[1] Department of Chemistry, HKU-CAS Joint Laboratory of New Materials, University of Hong Kong, Hong Kong SAR, China

[2] HKU Zhejiang Institute of Research and Innovation, Zhejiang 311305, China

[3] Center for Condensed Matter Sciences, National Taiwan University, Taipei, 10617, Taiwan

[4] Center of Atomic Initiative for New Materials, National Taiwan University, Taipei, 10617, Taiwan

[5] State Key Laboratory of Synthetic Chemistry, University of Hong Kong, Hong Kong SAR, China

[6] These authors contributed equally: Xiaoyong Mo and Yulin Deng

[*] Corresponding authors. HYAY: hoyuay@hku.hk; ECMT: ecmtse@hku.hk

Keywords

Mechanical Bond, Copper Catenane Complex, Oxygen Reduction, Molecular Electrocatalysis, Ligand Interlocking

Abstract

Efficient O_2 reduction reaction (ORR) for selective H_2O generation enables advanced fuel cell technology. Non-precious metal (NPM) catalysts are viable and attractive alternatives to state-of-the-art Pt-based materials that are expensive. Cu complexes inspired by Cu-containing O_2 reduction enzymes in nature have yet to reach their desired ORR catalytic performance. Here, the concept of mechanical interlocking is introduced to the ligand architecture to enforce dynamic spatial restriction on the Cu coordination site unachievable using other structural means. The utility of the kinetic effects from mechanical bond in transition metal catalysis is just about to emerge, and here the catenane ligands govern the O_2 adduct binding mode, thereby steering the selectivity to generate H_2O as the major product via the $4e^-$ pathway, rivaling the selectivity of Pt. The kinetic effects from the interlocked catenane ligand also promotes product elimination and boosts the onset potential by 130 mV, the mass activity by 1.8 times, and the turnover frequency (TOF) by 1.5 folds as compared to the non-interlocked counterpart. Our Cu catenane complex represents one of the first examples to take advantage of mechanical interlocking to afford electrocatalysts with enhanced activity and selectivity. The mechanistic insights gained through this integrated experimental and theoretical study are envisioned to be of practical value not just to the area of ORR energy catalysis, but also with broad implications on interlocked metal complexes that are of critical importance to the general fields in redox reactions involving proton-coupled electron transfer (PCET) steps.

Introduction

Catalysts for efficient energy conversion are of fundamental importance for sustainable development due to the pressing need for clean energy source and new green technologies.[1-5] In particular, fuel cell represents an alternative technology to directly utilize chemically stored energy in fuels with theoretical efficiency about thrice higher than conventional combustion engines.[6-7] Performance of low-temperature polymer electrolyte membrane (PEM) fuel cells has yet to reach

practical levels and the major challenge underlying the development of an efficient PEM fuel cells lies in the oxygen reduction reaction (ORR) occurring at the cathode.[8-10] Due to the high ORR activation barrier, state-of-the-art platinum-based electrocatalysts still exhibit high overpotentials (ca. 300 mV) and slow reaction kinetics.[11-13] A greater amount of the platinum catalyst is used at the cathode relative to that at the anode, thereby significantly increasing the cost due to the scarcity of the noble metal.[14-18] Development of low-cost electrocatalysts derived from earth-abundant metals for efficient ORR is therefore of crucial importance in providing a sustainable solution to clean and efficient energy conversion.[8, 19-24]

ORR is a complex inner-sphere process involving four electrons and four protons, and the intricate proton-coupled electron transfer (PCET) mechanism renders catalyst materials derived from base metals a low selectivity with the concomitant generation of deleterious H_2O_2 side-product.[25-29] On the other hand, oxygenases that employ iron or copper in their active sites for highly efficient and selective O_2 reduction and activation can serve as a valuable inspiration for designing molecular complexes that can overcome this activity-selectivity challenge.[30-34] While efforts have been devoted over the years to mimic the immediate coordination environment around the metal active site in metallo-oxygenases for efficient ORR, only limited success has been achieved even with sophisticated structural models.[35-37] In particular, capturing the kinetic and dynamic features beyond the immediate coordination sphere provided by the polypeptide backbone that folds into a highly elaborated 3D structure has been challenging through the use of structurally simple synthetic ligands.[38] The large size of the polypeptide backbones not only provide a dynamic framework with fast reorganization kinetics that enhances reactivity and stability, but the intricate polypeptide matrix also sterically controls the entry and orientation of substrate for tuning the selectivity and specificity of the metalloenzymes.[39]

Catenane is a class of mechanically interlocked molecules (MIMs) that consist of interlocked macrocycles.[40-41] Mechanical interlocking holds the catenane in place as a single molecule, and yet endows the interlocked macrocycles a high degree of motional freedom, and such unique features could be an effective mimic of the kinetic

features of metallo-oxygenases for developing molecular ORR catalysts (Fig. 1a). In this work, we report molecular copper catalysts featuring catenanes as the supporting ligands for efficient dioxygen reduction with tunable activity and selectivity (Fig. 1b). As the interlocked ligands in the catenane-supported catalysts are confined by the mechanical bond that limits the accessible ligand conformations around the metal when compared to that of non-interlocked counterparts, the required ligand rearrangement from ground state to transition state would be entropically more favorable and result in a higher catalyst activity. Substrate orientation could also be restricted by the mechanical bond with an enhanced product selectivity. Since complete ligand dissociation is prohibited by the mechanical bond, the active metal center is also protected from the attack of solvents and other competitive ligands with a stable resting state and long catalyst lifetime.[42] Yet, dynamic co-conformational change of the catenane could transiently open the metal coordination sphere for catalysis when being approached by the substrate, and that the intramolecular ligand re-coordination/rearrangement after substrate transformation could also facilitate product dissociation to result in a faster turnover. These favorable features concerning the kinetic aspect of catalysis thus pave the way to the development of mechanical interlocking as a new paradigm in designing transition metal catalysts. In fact, catenanes are promising scaffolds for catalyst developments,[42-44] and other aspects of MIMs such as large-amplitude co-conformational change and mechanostereochemistry have been exploited in switchable and stereoselective catalysis as well.[45-48]

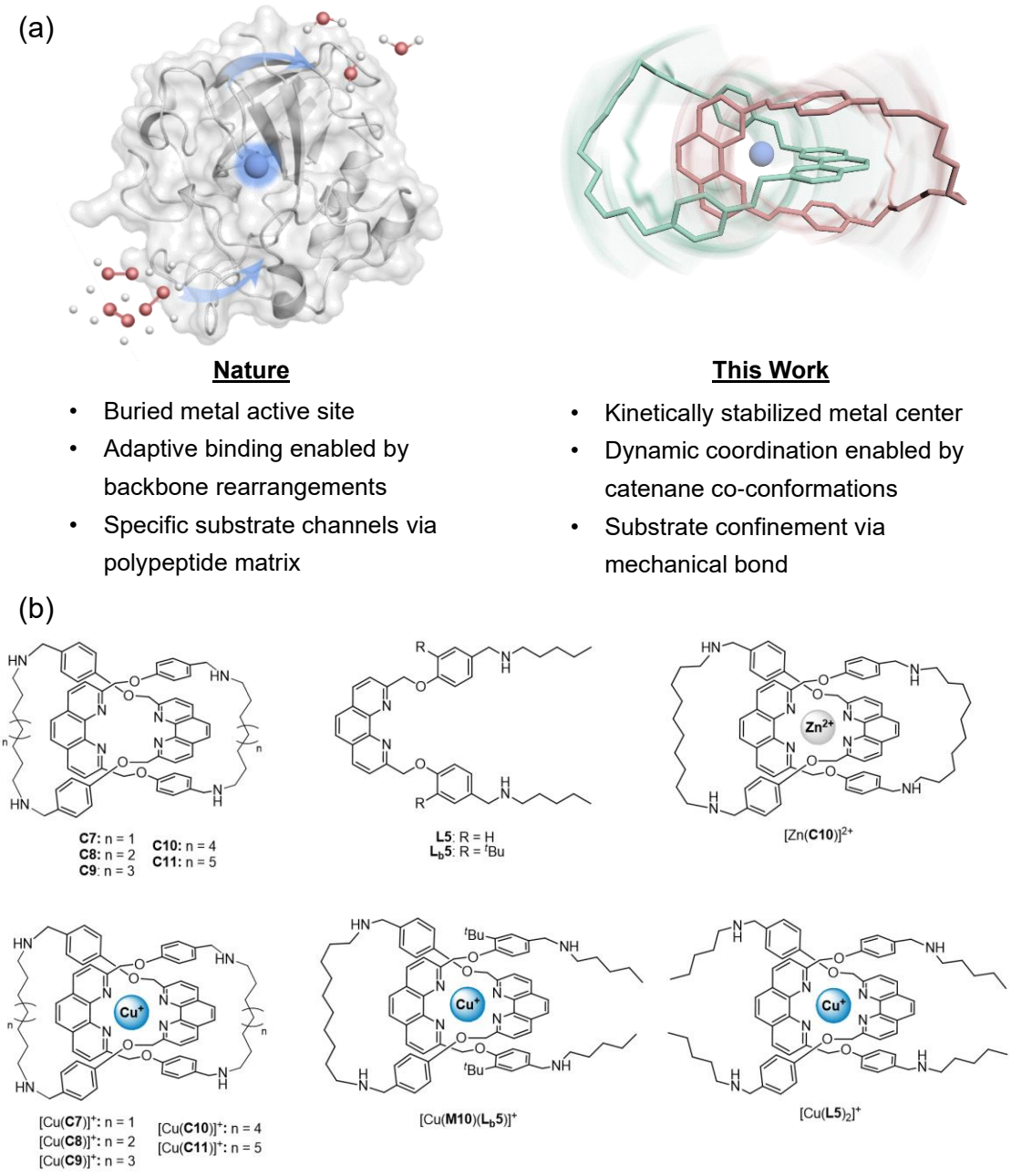

Figure 1. Mechanical interlocking as a new design principle for functional mimics of enzymes. (a) Concept of mimicking metalloenzyme backbone dynamics using mechanically interlocked molecular inorganic compounds (MIMICs). (b) Structures of Cu catenanes and non-interlocked control compounds used in this study.

Results and Discussion

Development of Mechanically Interlocked Catalysts. Catenane complexes of Cu(I) with a bis(phenanthroline) coordination (i.e. [Cu(**C7**)]$^+$, [Cu(**C8**)]$^+$, [Cu(**C9**)]$^+$, [Cu(**C10**)]$^+$, and [Cu(**C11**)]$^+$) were selected as an entry point in this work to mimic the

kinetic features of peptide backbones in enzymes (see SI Section 1). These catenane ligands can be efficiently prepared in gram-scale from the well-studied Cu(I) templated synthesis,[42, 49] and they contain aliphatic linkers of different lengths for controlling the tightness of the mechanical bond. The bis(phenanthroline) Cu(I) is coordinatively saturated that gives a stable resting state, and the coordination sphere will need to open in order to accept the incoming O_2. These catenanes with varying degrees of mechanical bond tightness will therefore enable a systematic investigation on the effects of ligand reorganization kinetics on the ORR activity. Although similar copper(I) catenanes have first been synthesized,[50-51] and that the effects of the mechanical bond on their kinetic stability against oxidation and ligand substitution has been identified about 30 years ago,[52-54] it is not until recently that these unique kinetic features of catenanes have been applied in developing copper-catalyzed organic reactions.[42]

One challenge in the rational design of molecular ORR catalysts is that ligand exchange during physisorption may lead to an active catalyst on the electrode different from that prepared and characterized in solutions. The exceptional stability of catenane complexes would therefore result in a high structural fidelity of the catalysts in different conditions and physical states. The X-ray crystal structure of $[Cu(\mathbf{C8})]^+$ shows a 4-coordinate Cu(I) center supported by four nitrogen donors from the two phenanthrolines with Cu–N bond lengths of 2.016(5) Å – 2.032(5) Å in a tetrahedral coordination geometry, where a dihedral angle of 87.3° is found between the two phenanthroline planes (Fig. 2a and Tables S1). The structure of $[Cu(\mathbf{C10})]^+$ shown in Fig. S1 is similar to that of $[Cu(\mathbf{C8})]^+$ except the longer alkyl linkers in the former are more disordered and conformationally flexible. The Cu–N bond lengths are found to be 2.008(5) Å – 2.043(6) Å and a dihedral angle of 88.1° is observed between the two phenanthrolines, suggesting that the different alkyl linkers have minimal effects on the equilibrium structure around the coordination sphere. The Cu(I) catenane complexes are physisorbed onto porous carbon supports (see SI Section 2) to enable interfacial electrocatalysis. X-ray absorption near edge structure (XANES) spectrum of Vulcan-supported $[Cu(\mathbf{C10})]^+$ shows that Cu(I) is the dominant form

when the complex is physisorbed on heterogeneous carbon surfaces (Fig. 2b), while the extended X-ray absorption fine structure (EXAFS) spectrum shows that the Cu-N atomic interactions (2.00 Å) in the complex dispersed on porous carbon matrices match the Cu-N bond lengths in the corresponding crystal structure (Fig. 2c, Fig. S2, and Tables S2-S3). XANES and EXAFS results further demonstrate that the Cu oxidation state and core coordination geometry of $[Cu(\mathbf{C10})]^+$ are similar to those of the non-interlocked control compound $[Cu(\mathbf{L5})_2]^+$ at equilibrium (Fig. 2b, 2c), likely hinting that differences observed in their catalytic performances (*vide infra*) are of kinetic, not thermodynamic, in nature. $[Cu(\mathbf{C10})]^+$ displays a Cu(I/II) redox wave at 0.79 mV vs NHE (Fig. S3-S4), suggesting that the complex could reduce O_2 at favourable onset potentials by accessing Cu(I) readily. Taken together, Cu catenane complexes on heterogenous surfaces are electrochemically active and structurally similar to their pristine molecular forms.

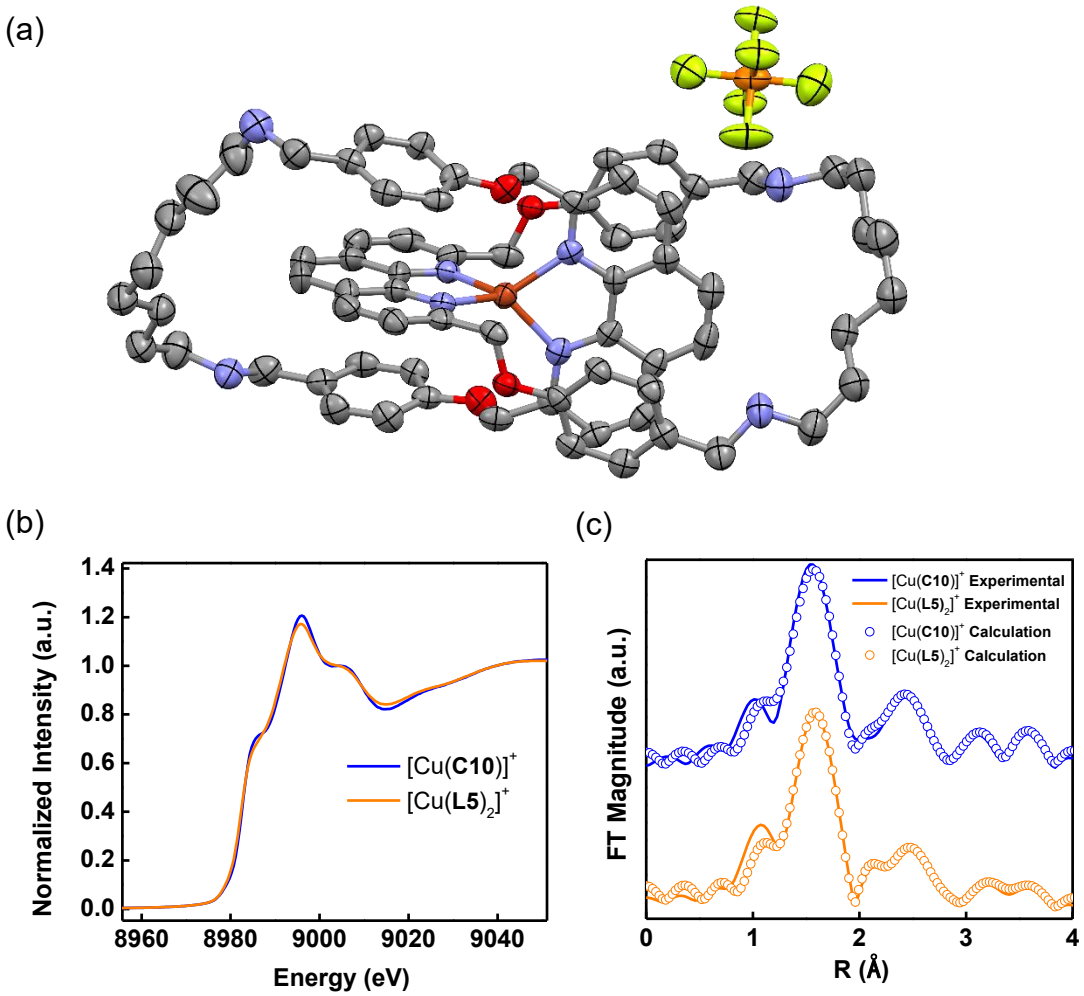

Figure 2. X-ray crystal structure and absorption spectroscopy of Cu(I) catenane and non-interlocked complexes. (a) Molecular structure of [Cu(**C8**)]PF_6 with anisotropic displacement ellipsoids set at 50% probability level. Solvent molecules and hydrogen atoms are omitted for clarity. (Brown: Cu; Blue: N; Red: O; Grey: C; Orange: P; Lime: F) (b) Cu K-edge XANES spectra and (c) Fourier transformed EXAFS (k^3-weighted) spectra (line) and fitting results (dot) of [Cu(**C10**)]$^+$ (blue) and [Cu(**L5**)$_2$]$^+$ (orange) supported on carbon.

ORR Investigation

Effect of Mechanical Interlocking on ORR Performance. Rotating ring-disk electrode (RRDE) experiments were carried out to investigate how mechanical interlocking improves the electrocatalytic performance of the Cu complexes. Fig. 3a shows the linear sweep voltammograms (LSVs) of [Cu(**C7**)]$^+$, [Cu(**C8**)]$^+$, [Cu(**C9**)]$^+$, [Cu(**C10**)]$^+$, and [Cu(**C11**)]$^+$ supported on Vulcan carbon in O_2-saturated pH 7 buffer. Intriguingly, [Cu(**C10**)]$^+$ displays the largest ORR disk current density (Fig. 3a), the

most positive ORR onset potential (Fig. 3b), and the highest selectivity for H_2O (Fig. 3c) among the five Cu catenanes with varying linker lengths in both neutral and alkaline media (Fig. S5), suggesting that the tightness and co-conformational dynamics of the catenanes can alter electrocatalytic attributes of molecular complexes. Upon lengthening the linker from **C7** to **C10**, the ORR onset potential increases while the selectivity for H_2O enhances. Upon extending the linker length from **C10** to **C11**, ORR proceeds via a substantial overpotential to produce deleterious H_2O_2 byproduct. The ORR attributes of our best-performing [Cu(**C10**)]$^+$ are more favorable than those of Cu complexes with 2,2'-dipicolylamine (DPA) and 1,10-phenanthroline (phen) as well as can rival those of state-of-the-art artificial molecular Cu complexes featuring 2,9-Et_2-phen and tris(2-pyridylmethyl)amine ligands (Table S4).[32, 55-58]

The observed trend in the ORR activity and selectivity could be explained by the size of the accessible conformational space of the ligands upon mechanical interlocking. From [Cu(**C11**)]$^+$ to [Cu(**C10**)]$^+$, a smaller size of the interlocked rings will reduce the number of accessible ligand conformations around the Cu ion, and therefore result in a lower entropic cost in ligand re-organization for O_2 binding and orientation of subsequent intermediates, and thus enhancing overall ORR activity and selectivity. Upon further constricting the catenane size from [Cu(**C10**)]$^+$ to [Cu(**C7**)]$^+$, ligand re-organization in a smaller accessible conformational space would however limit the Cu centre to be fully approachable by the substrate in the orientation for optimal ORR activity and selectivity. These behaviours of catenane ligands are reminiscent to natural systems where protein dynamic motions and transient conformations are necessary for enzyme activity.[30-31, 35-37, 39, 59-61]

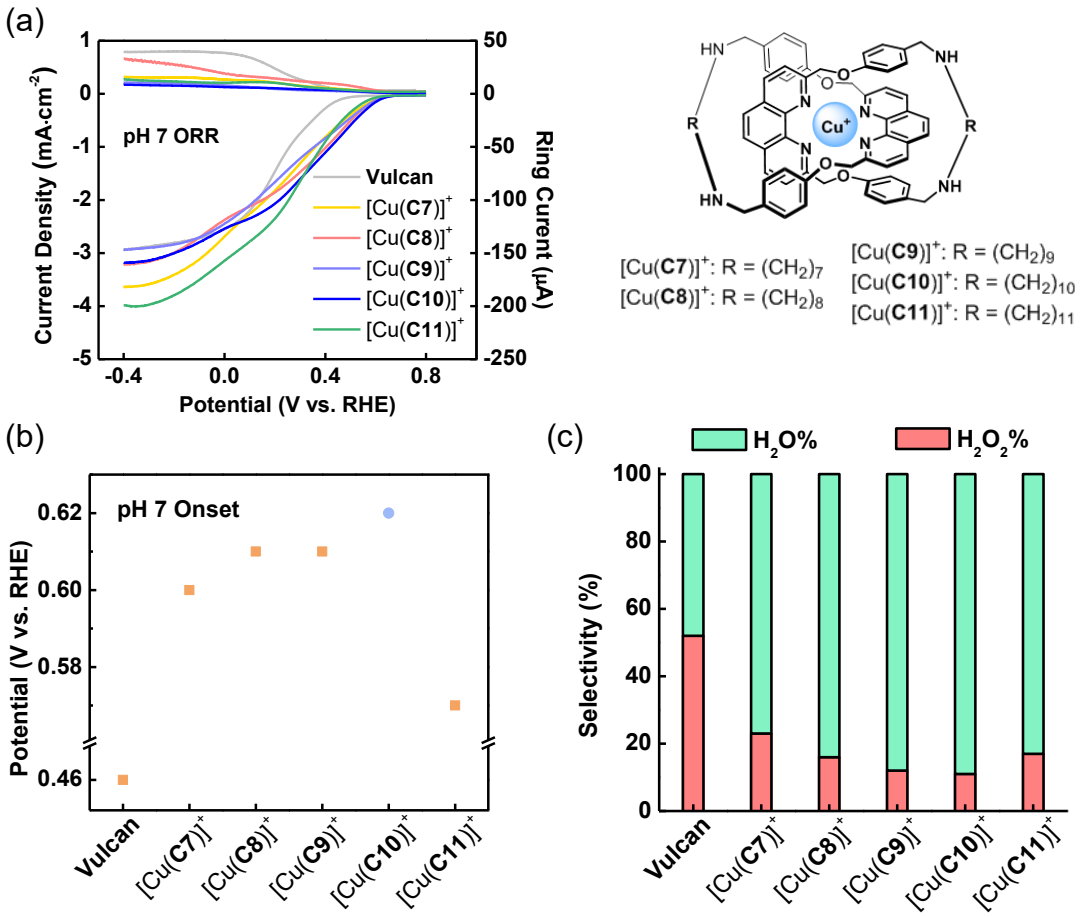

Figure 3. Impact of mechanical bond tightness on the electrocatalytic performance of Cu catenanes. (a) ORR linear sweep voltammograms (LSVs) with disk and ring currents, (b) ORR onset potentials, and (c) ORR product selectivity at 0.15 V vs. RHE in pH 7 catalyzed by Vulcan carbon (gray), [Cu(**C7**)]$^+$ (yellow), [Cu(**C8**)]$^+$ (red), [Cu(**C9**)]$^+$ (lilac), [Cu(**C10**)]$^+$ (blue), and [Cu(**C11**)]$^+$ (green).

Effect of Mechanical Interlocking on ORR Onset Potential. The ORR performance of [Cu(**C10**)]$^+$ is further explored by comparing the electrocatalytic metrics of [Cu(**C10**)]$^+$ with redox-inactive control compounds including phenanthroline ligand **L5**, catenane ligand **C10**, and Zn(II) catenane complex [Zn(**C10**)]$^{2+}$. Fig. 4a and S6a show LSVs of the disk and ring currents of ORR catalyzed by our catalysts in neutral and basic conditions. The first metric to consider is the ORR onset potential and overpotential. Fig. 4b and Fig. S6b summarize the ORR onset potentials of our catalysts in pH 7 and 13. Under both pH conditions considered, [Cu(**C10**)]$^+$ displays the most positive onset potential among the catalysts

tested. [Cu(**C10**)]$^{+}$ show significantly more favourable onset potential when compared to the **L5**, **C10**, and [Zn(**C10**)]$^{2+}$, supporting that the Cu ion coordinated to the catenane is the origin of the ORR activity of [Cu(**C10**)]$^{+}$.

Effects of the catenane structure on ORR are further investigated by comparing with [Cu(**L5**)$_2$]$^{+}$ and [Cu(**M10**)(**L$_b$5**)]$^{+}$, which are the closest non-interlocked and (pseudo)rotaxane analogues of [Cu(**C10**)$_2$]$^{+}$ respectively containing pentyl side chains and a decamethylene linker in the linear and macrocyclic phenanthroline ligands. Intriguingly, [Cu(**C10**)]$^{+}$ exhibits an onset potential 130 mV more positive than that of the non-interlocked [Cu(**L5**)$_2$]$^{+}$, indicating that mechanical interlocking can lower the activation barrier for ORR. The onset potential displayed by the rotaxane complex [Cu(**M10**)(**L$_b$5**)]$^{+}$ is in between those of [Cu(**C10**)]$^{+}$ and the non-interlocked [Cu(**L5**)$_2$]$^{+}$, which is in line with the less tight mechanical bond of rotaxane than catenane with comparable interlocked components. Shrinking the electrochemical activation barrier of ORR is one of the holy grails in the field of low-temperature PEM fuel cells, and here we demonstrate that upon mechanical interlocking the coordinating ligands as catenanes, the driving force needed to jump start ORR can be minimized.

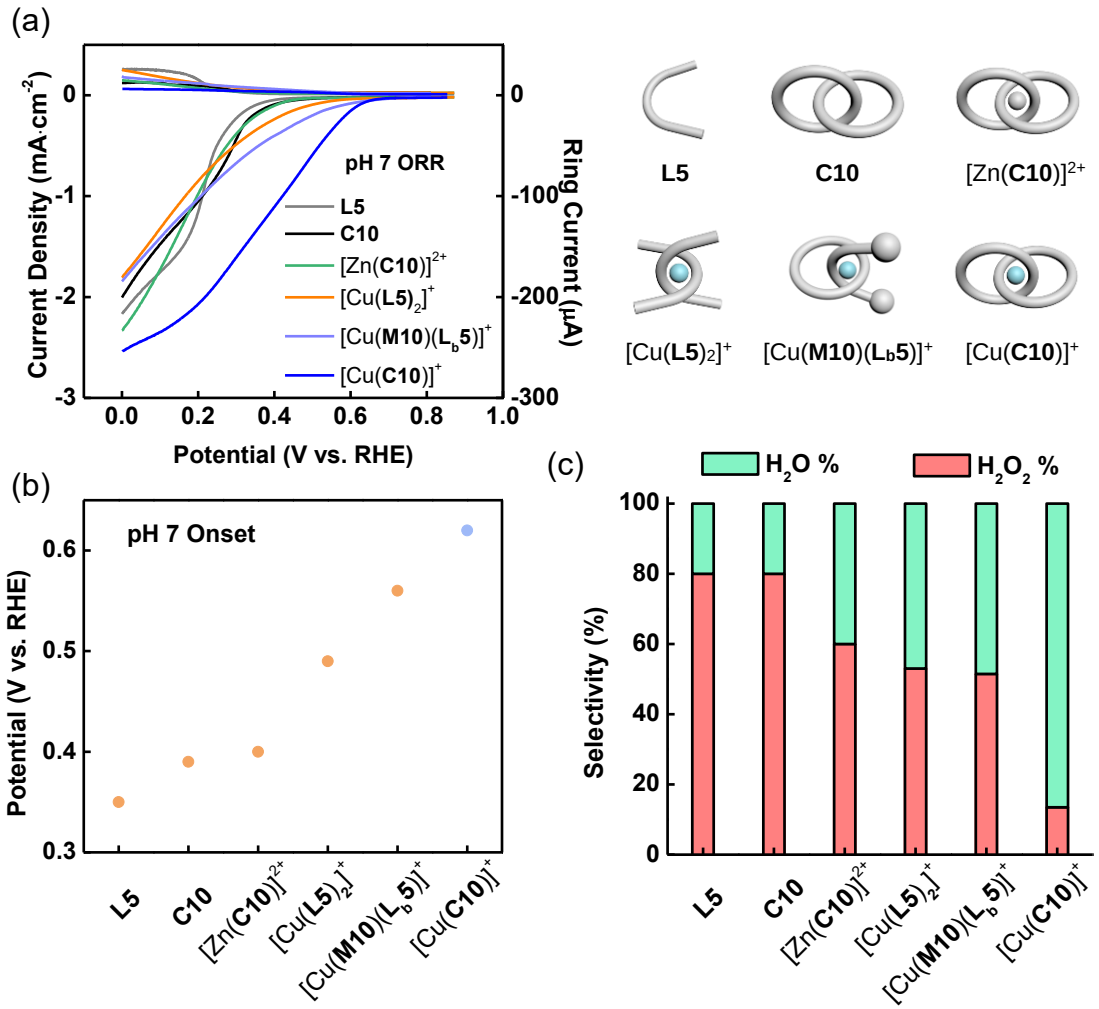

Figure 4. Performance metrics of mechanically interlocked molecular inorganic catalysts and control compounds. (a) ORR LSVs with disk and ring currents, (b) ORR onset potentials, and (c) ORR product selectivity at 0.15 V vs RHE in pH 7 catalyzed by of **L5** (gray), **C10** (black), [Zn(**C10**)]$^+$ (green), [Cu(**L5**)$_2$]$^+$ (orange), [Cu(**M10**)(**L**$_b$**5**)]$^+$ (lilac), and [Cu(**C10**)]$^+$ (blue).

Effect of Mechanical Interlocking on ORR Product Selectivity. ORR product selectivity, another key electrocatalytic performance indicator, of our catalysts is next explored in pH 7 and 13 (Fig. 4c and S6c). At both the kinetically controlled and diffusion limited regions, the mechanically interlocked [Cu(**C10**)]$^+$ displays the highest selectivity (ca. 90%) for the 4e$^-$ pathway to generate H_2O as the product. By contrast, the rotaxane complex [Cu(**M10**)(**L**$_b$**5**)]$^+$ and non-interlocked [Cu(**L5**)$_2$]$^+$ generate significant amounts of H_2O_2 through the 2e$^-$ pathway (H_2O_2 selectivity > 50%). Taken together, these results corroborate that interlocking the ligands as a

catenane could direct the orientation of the O_2 adduct that promotes O–O bond cleavage, leading to the production of environmentally benign H_2O via a $4e^-$ pathway, whereas the less restricted (pseudo)rotaxane and non-interlocked ligand framework could retain the O–O bond and releases H_2O_2 as deleterious by-product via a $2e^-$ pathway.

Effects of Mechanical Interlocking on ORR Mass Activity and Turnover Frequency (TOF). We next investigate how mechanical interlocking can benefit ORR electrocatalysis in terms of mass activity. ICP-MS was conducted to quantify the metal content in the Cu complexes (Fig. S7 and Table S5). Fig. 5a and S8a display the mass activities of $[Cu(\mathbf{C10})]^+$ and $[Cu(\mathbf{L5})_2]^+$ with their ORR current densities normalized by their Cu quantity. Across all the pH values studied, $[Cu(\mathbf{C10})]^+$ displays higher ORR activity on a per mass basis relative to the non-interlocked $[Cu(\mathbf{L5})_2]^+$ by 1.8 times, suggesting that the catenane ligand promotes faster ORR rates per single Cu site. This result can likely be rationalized by the faster ligand reorganization kinetics due to mechanical interlocking as a means to lower the ORR activation barrier as well as remove H_2O from the Cu center and to expose open coordination site for fresh O_2, thereby facilitating both product release and reactant engagement.

Another electrocatalytic performance metric of importance is turnover frequency (TOF). Fig. 5b and S8b show the TOF of $[Cu(\mathbf{C10})]^+$ and $[Cu(\mathbf{L5})_2]^+$ in pH 7 and 13 utilizing information collected from previous sections. In both neutral and basic environments examined, the catenane-supported $[Cu(\mathbf{C10})]^+$ exhibits TOF values higher than the non-interlocked $[Cu(\mathbf{L5})_2]^+$ by 1.5 folds, suggesting that the Cu complex with a mechanically interlocked ligand set facilitates the rate-determining step (RDS) of ORR at a higher efficiency as compared with the Cu complex with higher flexibility in coordination geometry. This observation can be rationalized by the differences in selectivity and mass activity between $[Cu(\mathbf{C10})]^+$ and $[Cu(\mathbf{L5})_2]^+$. Our result demonstrates that the mechanically interlocked $[Cu(\mathbf{C10})]^+$ has a higher tendency to promote the $4e^-$ pathway while exhibiting higher ORR rate per Cu active

site.

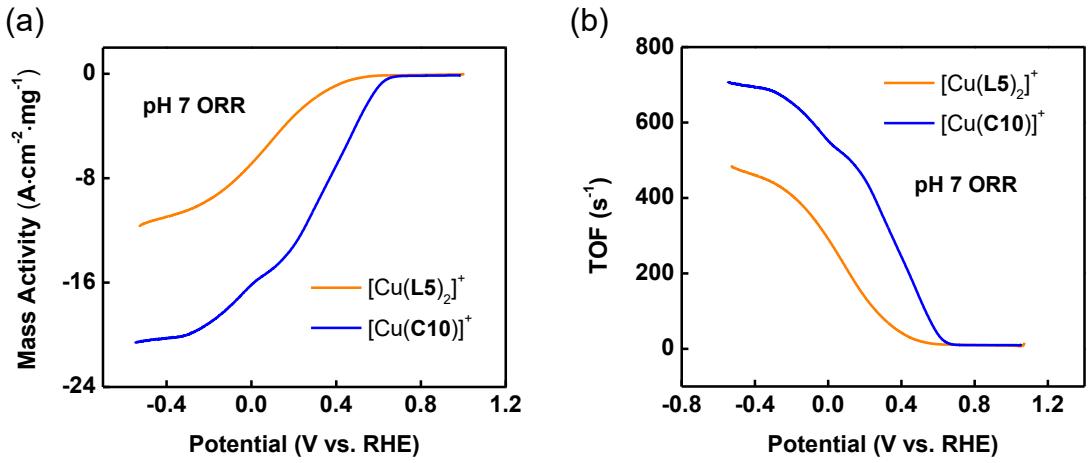

Figure 5. Kinetic enhancement imbued by mechanical interlocking. (a) Mass activity and (b) turnover frequency (TOF) of [Cu(**C10**)]$^+$ (blue) and [Cu(**L5**)$_2$]$^+$ (orange) with their ORR current densities in pH 7 normalized by their Cu quantity.

Effect of Mechanical Interlocking on ORR Pathway and Catalytic Rate. After establishing the relationship between mechanical interlocking and enhanced catalytic activity as well as optimized product selectivity, more mechanistic detail at the molecular level is further explored. First, the number of electrons transferred during the RDS was deduced using Tafel analysis. The Tafel slopes of [Cu(**C10**)]$^+$ and [Cu(**L5**)$_2$]$^+$ were found to be 119 and 247 mV/dec, respectively (Fig. S9). Kinetic isotope effect (KIE) studies were subsequently conducted to gain insight into the role of protons in the ORR pathway. In all cases, upon deuteration, the ORR onset potential is shifted in the negative direction, the ORR current density decreases, the peroxide yield increases, and the Tafel slope increases (Fig. S10). These results together indicate that protons are involved at or before the rate-determining step (RDS) of ORR on [Cu(**C10**)]$^+$ and [Cu(**L5**)$_2$]$^+$.

DFT Calculations for Further Understanding of Mechanical Bond Effects on O_2 Binding, H_2O Product Release, and ORR Pathway Selectivity. Further insights into the functional roles of the catenane ligand on O_2 binding was investigated by DFT calculations using a 6-31+G**/LANL2DZ(Cu) mixed basis set and B3LYP

exchange-correlation functional. Upon O_2 binding, the Cu-bound O_2 adducts and intermediates derived from the addition of an O_2 molecule was computed (Fig. S11). ORR catalytic cycles of $[Cu(\mathbf{C10})]^+$ and $[Cu(\mathbf{L5})_2]^+$ were constructed based on optimized structures and calculated energies (Fig. S12-S13). The simulated resting state structure of $[Cu(\mathbf{C10})]^+$ matches its X-ray crystal structure in Fig. 2a. As shown in Fig. 6, O_2 coordination to Cu(I), the first step of ORR, is thermodynamically unfavorable with a positive ΔG for both $[Cu(\mathbf{C10})]^+$ and $[Cu(\mathbf{L5})_2]^+$. Comparing the initial O_2 coordination step, the catenane complex $[Cu(\mathbf{C10})]^+$ was found to have a significantly less positive ΔG of 29.7 kcal mol^{-1} (ΔH: 28.3 kcal mol^{-1}; $T\Delta S$: -1.5 kcal mol^{-1}) in contrast to the 44.1 kcal mol^{-1} for $[Cu(\mathbf{L5})_2]^+$ (ΔH: 38.1 kcal mol^{-1}; $T\Delta S$: -6.0 kcal mol^{-1}), which is consistent with the higher catalytic activity observed for the catenane complex. The lower entropic penalty upon O_2 binding suggests that the catenane complex requires less ligand reorganization during ORR. Fig. S12-S13 further show that the last step of H_2O product release from the catenane complex is more favourable than that from the non-interlocked complex by 0.08 V, further supporting the higher ORR activity observed for the catenane complex.

A closer analysis of the structure of the first Cu-bound O_2 intermediate showed that the **C10**-supported complex has a side-on coordinated O_2 with a O–O bond length of 1.31 Å, whereas the coordinated O_2 in the non-interlocked complex supported by **L5** has an end-on coordination geometry with an O–O bond length of 1.27 Å (Fig. S11). The slightly longer O–O bond length in $[Cu(\mathbf{C10})(O_2)]^+$ may suggest a higher degree of O_2 activation as a result of the better orbital overlap between the copper and the η^2-coordinated O_2, which could also explain the more favorable ΔH for the catenane-supported complex.

On the other hand, the different coordination geometries for the bound O_2 in the interlocked and non-interlocked catalysts are also likely a result of the different extent of reorganization of the copper coordination sphere during the course of O_2 binding (Fig. 6). Since the two phenanthrolines in $[Cu(\mathbf{C10})]^+$ are mechanically interlocked and their conformations are more restricted, there is a lower entropic cost in reorganizing the coordination sphere to accept the incoming O_2. Furthermore, it has

been reported that a side-on coordination mode promotes O–O bond cleavage to give H_2O as the product, whereas an end-on O_2 binding mode likely generates H_2O_2 without a complete O–O bond cleavage. Taking together these mechanistic insights, the O–O bond cleavage step is likely the selectivity-governing step (SGS). All in all, our comparative experimental and computational results show that mechanical interlocking can steer ORR down a $4e^-$ pathway to generate H_2O exclusively as the desired product with high efficiency.

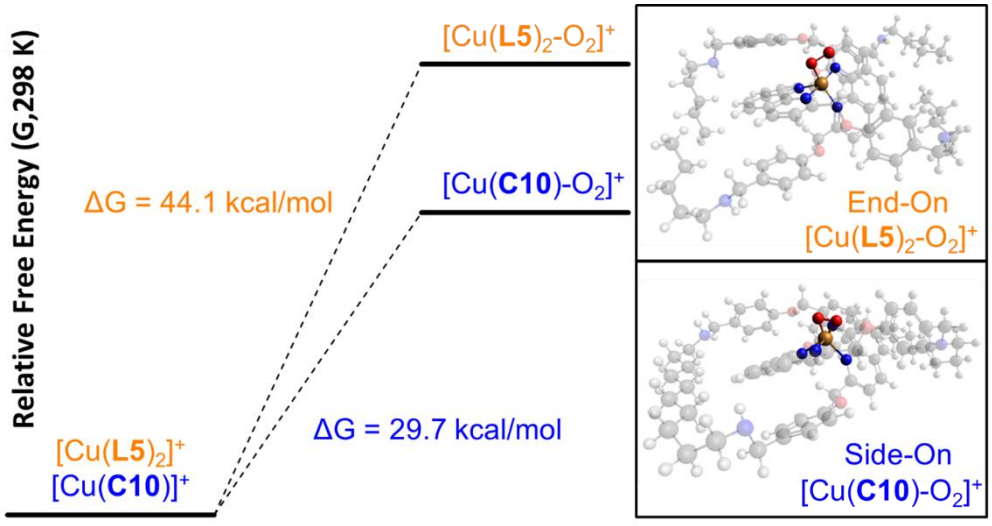

Fig. 6 | Free energy calculations of O_2 activation by mechanically interlocked and non-interlocked complexes. Change in O_2 binding mode of [Cu(**C10**)]$^+$ and [Cu(**L5**)$_2$]$^+$ at 6-31+G**/LANL2DZ(Cu) level. (Orange: Cu, Red: O, Blue: N, Grey: C, White: H)

Conclusions

Mechanical interlocking provides a new direction to restrict molecular motion, thereby enabling excellent catalytic turnovers and product selectivity in transition metal catalysis. Here, the as-synthesized catenane-supported [Cu(**C10**)]$^+$ and non-interlocked [Cu(**L5**)$_2$]$^+$ were characterized using single crystal X-ray diffraction as well as X-ray absorption spectroscopy techniques and subsequently tested for their ORR performance. Intriguingly, upon mechanical interlocking the ligands as a catenane, the ORR onset potential, mass activity, H_2O selectivity, and electrocatalytic

TOF all improved significantly under neutral and basic conditions. Through combined experimental techniques and theoretical calculations, O_2 adduct binding mode was found to hasten the rate-determining step and steer the selectivity-governing step to produce H_2O efficiently as the major product. The mechanistic insights gained from this ORR study and the concept of precise regulation of the size of the accessible ligand conformational space upon mechanical interlocking are readily applicable to other redox processes involving multiple PCET steps that are central to the development of advanced energy catalysis schemes.

Methods

General Methods. Chemicals for synthesis were obtained from commercial sources and used as received unless otherwise stated. Electrochemical studies at pH 7 were performed in Britton-Robinson buffer (BR) containing H_3BO_3 (0.04 M, 99.999%, Fisher Scientific), CH_3COOH (0.04 M, 100%, VWR), H_3PO_4 (0.04 M, 85 wt% in H_2O, J&K Scientific), and $NaClO_4$ (0.1 M, 99.9%, Sigma-Aldrich). The solution pH was adjusted to 7 using NaOH (10 M, analytical grade, Merck Millipore). Experiments at pH 13 were performed in 100 mM NaOH (analytical grade, Merck Millipore) diluted with Milli-Q ultrapure water (> 18.2 MΩ·cm).[62] Solutions were sparged with O_2 (99.995% high purity grade, Linde HKO) for 30 min before each experiment following published methods.[63-66]

Electrochemical Activity Measurements. The ORR activity of the prepared samples was measured using a rotating ring-disk electrode (RRDE) in a three-compartment electrochemical cell with an aqueous "no-leak" Ag/AgCl (3 M KCl, EDAQ Inc). A graphite rod served as a counter electrode separated from the working electrode by a glass frit. RRDE electrochemical experiments were conducted using a CH Instruments 760E bipotentiostat and a Pine Instruments WaveVortex Electrode Rotator. The working electrode was a glassy carbon disk (A = 0.196 cm^2) with a Pt ring (A = 0.093 cm^2, Pine Instruments, cleaned using an electrochemical method by cycling from -0.4 V to 1.7 V vs. Ag/AgCl in 100 mM $HClO_4$ solution). Electrochemical

potentials were reported relative to the reversible hydrogen electrode (RHE) using published protocols.[57] The ring potential was held at 1.23 V vs. RHE during RRDE experiments to oxidize peroxide into oxygen efficiently. Ring electrode collection efficiency was calculated from the current response of Fe^{3+}/Fe^{2+} redox couple of 5 mM $K_3Fe(CN)_6$ in 100 M KCl. The RRDE collection efficiency (N_c) was determined to be 22.96% using *Eq 1*,[67]

$$N_c = \left| \left(\frac{i_{r,Fe^{2+/3+}}}{i_{d,Fe^{2+/3+}}} \right) \left(\frac{n_d}{n_r} \right) \right| \qquad (1)$$

where $i_{r,Fe2+/3+}$ and $i_{d,Fe2+/3+}$ are defined as the ring and disk limiting currents in the presence of $K_3Fe(CN)_6$, respectively. n_d and n_r are the number of electrons exchanged at the disk and ring, respectively.

Subsequently, the number of electrons transferred per O_2 during ORR (n_{RRDE}) can be calculated from $i_{d,ORR}$, $i_{r,ORR}$, and N_c using *Eq 2*,[68]

$$n_{RRDE} = 4 \times \frac{i_{d,ORR}}{i_{d,ORR} + \frac{i_{r,ORR}}{N_c}} \qquad (2)$$

where $i_{r,ORR}$ and $i_{d,ORR}$ refer to the ring and disk currents during ORR assessment, respectively.

Molecular Characterization. X-ray absorption spectroscopy (XAS) measurements were conducted in transmission mode using the TLS beam line 17C at the National Synchrotron Radiation Research Center (NSRRC), Hsinchu, Taiwan. All spectra were normalized and analyzed with the Athena and Artemis software.[69] Extended X-ray absorption fine structure (EXAFS) data were weighted by k^3 to compensate for damping at the high k region. Fourier transformed (FT) EXAFS data were presented with photoelectron phase correction. Local structure parameters (i.e. bond length and Debye-Waller factor) were obtained through nonlinear least square curve fitting of the EXAFS spectra. Nonlinear EXAFS curve fitting was performed in the range of 1~4 Å in r-space.

Computational Methods. Density functional theory (DFT) calculations were carried

out with Gaussian 09 (revision D.01)[70] after building the molecules using the Avogadro software.[71] Geometry optimizations and single-point energy calculations of all structures were done using the spin-unrestricted hybrid density functional B3LYP.[72-74] Similar to previous studies on copper complexes,[75-77] a mixed basis set with LANL2DZ on Cu and 6-31G (d,p) on all remaining atoms.[78-79] Solvation by water (ε = 78.3553) was accounted for using the polarizable continuum model (PCM).[80] In the structural optimization step, a 10^{-8} convergence criterion in the density matrix was applied and vibrational analyses have also been carried out for validation. To construct the intrinsic reaction coordinates (IRC) and the catalytic cycle of the oxygen reduction with [Cu(**C10**)]$^+$ and [Cu(**L5**)$_2$]$^+$, the changes in free energy (ΔG), enthalpy (ΔH), and entropy (ΔS) in all intermediate steps were calculated using the difference in total free energy (G), enthalpy (H), and entropy (S) between products and reactants respectively:

For all processes that only involve electron transfer, the reduction potential $E°$ was calculated using the Nernst Equation (*Eq 3*):

$$E^o = \frac{-\Delta G^o}{nF} - E_{SHE} \qquad (3)$$

where ΔG^o is the free energy of the reaction calculated previously. n represents the number of electrons transferred during the reaction of interest, F is the Faraday constant, E_{SHE} is the absolute potential of the aqueous standard hydrogen electrode (SHE), with the value of 4.24 V.

For processes involving single proton and electron transfer, the reduction potential $E°$ (at pH = 7) was calculated using *Eq 4*:

$$E^o = \frac{-[\Delta G^o - \frac{1}{2} G_f^o(H_2) - nRTln(10^{-7})]}{nF} - E_{SHE} \qquad (4)$$

where $G_f^o(H_2)$ is the formation energy of H_2 at standard conditions. R is the ideal gas constant (8.3145 $Jmol^{-1}K^{-1}$) and T is room temperature (298 K).

Analyses and visualization of optimized structures were performed using Chimera (version 1.12).[81]

Data availability

The experimental data, as well as the characterization data for all of the compounds prepared in the course of these studies, are provided in the Supplementary Information. The crystallographic data for the structures reported in this article have been deposited at the Cambridge Crystallographic Data Centre, under accession numbers: 2035988 for [Cu(**C8**)]PF_6 and 2050046 for [Cu(**C10**)]PF_6 (see the X-ray crystallographic data in the Supplementary Information). Copies of the data can be obtained free of charge via https://www.ccdc.cam. ac.uk/structures/.

References

(1) Dey, S.; Mondal, B.; Chatterjee, S.; Rana, A.; Amanullah, S.; Dey, A., Molecular electrocatalysts for the oxygen reduction reaction. *Nat. Rev. Chem.* **2017,** *1* (12), 0098.

(2) Strmcnik, D.; Kodama, K.; van der Vliet, D.; Greeley, J.; Stamenkovic, V. R.; Marković, N. M., The role of non-covalent interactions in electrocatalytic fuel-cell reactions on platinum. *Nat. Chem.* **2009,** *1* (6), 466-472.

(3) Kumar, A.; Ciucci, F.; Morozovska, A. N.; Kalinin, S. V.; Jesse, S., Measuring oxygen reduction/evolution reactions on the nanoscale. *Nat. Chem.* **2011,** *3* (9), 707-713.

(4) Zheng, Y.-R.; Vernieres, J.; Wang, Z.; Zhang, K.; Hochfilzer, D.; Krempl, K.; Liao, T.-W.; Presel, F.; Altantzis, T.; Fatermans, J.; Scott, S. B.; Secher, N. M.; Moon, C.; Liu, P.; Bals, S.; Van Aert, S.; Cao, A.; Anand, M.; Nørskov, J. K.; Kibsgaard, J., et al., Monitoring oxygen production on mass-selected iridium–tantalum oxide electrocatalysts. *Nat. Energy* **2022,** *7* (1), 55-64.

(5) Cheng, F.; Shen, J.; Peng, B.; Pan, Y.; Tao, Z.; Chen, J., Rapid room-temperature synthesis of nanocrystalline spinels as oxygen reduction and evolution electrocatalysts. *Nat. Chem.* **2011,** *3* (1), 79-84.

(6) Jaouen, F.; Proietti, E.; Lefèvre, M.; Chenitz, R.; Dodelet, J.-P.; Wu, G.; Chung, H. T.; Johnston, C. M.; Zelenay, P., Recent advances in non-precious metal catalysis for oxygen-reduction reaction in polymer electrolyte fuel cells. *Energy Environ. Sci.* **2011,** *4* (1), 114-130.

(7) Sun, Y.; Polani, S.; Luo, F.; Ott, S.; Strasser, P.; Dionigi, F., Advancements in cathode catalyst and cathode layer design for proton exchange membrane fuel cells. *Nat. Commun.* **2021,** *12* (1), 5984.

(8) Gewirth, A. A.; Varnell, J. A.; DiAscro, A. M., Nonprecious Metal Catalysts for Oxygen Reduction in Heterogeneous Aqueous Systems. *Chem. Rev.* **2018,** *118* (5), 2313-2339.

(9) Li, H.; Kelly, S.; Guevarra, D.; Wang, Z.; Wang, Y.; Haber, J. A.; Anand, M.; Gunasooriya, G. T. K. K.; Abraham, C. S.; Vijay, S.; Gregoire, J. M.; Nørskov, J. K., Analysis of the limitations in the oxygen reduction activity of transition metal oxide surfaces. *Nat. Catal.* **2021,** *4* (6), 463-468.

(10) Xie, X.; He, C.; Li, B.; He, Y.; Cullen, D. A.; Wegener, E. C.; Kropf, A. J.; Martinez, U.; Cheng, Y.; Engelhard, M. H.; Bowden, M. E.; Song, M.; Lemmon, T.; Li, X. S.; Nie, Z.; Liu, J.; Myers, D. J.; Zelenay, P.; Wang, G.; Wu, G., et al., Performance enhancement and degradation mechanism identification of a single-atom Co–N–C catalyst for proton exchange membrane fuel cells. *Nat. Catal.* **2020,** *3* (12), 1044-1054.

(11) Núñez, M.; Lansford, J. L.; Vlachos, D. G., Optimization of the facet structure of transition-metal catalysts applied to the oxygen reduction reaction. *Nat. Chem.* **2019,** *11* (5), 449-456.

(12) Wang, C.; Ma, L.; Liao, L.; Bai, S.; Long, R.; Zuo, M.; Xiong, Y., A unique platinum-graphene hybrid structure for high activity and durability in oxygen reduction reaction. *Sci. Rep.* **2013,** *3* (1), 2580.

(13) Li, J.; Alsudairi, A.; Ma, Z.-F.; Mukerjee, S.; Jia, Q., Asymmetric Volcano Trend in Oxygen Reduction Activity of Pt and Non-Pt Catalysts: In Situ Identification of the Site-Blocking Effect. *J. Am. Chem. Soc.* **2017,** *139* (4), 1384-1387.

(14) Greeley, J.; Stephens, I. E. L.; Bondarenko, A. S.; Johansson, T. P.; Hansen, H. A.; Jaramillo, T. F.; Rossmeisl, J.; Chorkendorff, I.; Nørskov, J. K., Alloys of platinum and early transition metals as oxygen reduction electrocatalysts. *Nat. Chem.* **2009,** *1* (7), 552-556.

(15) Hernandez-Fernandez, P.; Masini, F.; McCarthy, D. N.; Strebel, C. E.; Friebel, D.; Deiana, D.; Malacrida, P.; Nierhoff, A.; Bodin, A.; Wise, A. M.; Nielsen, J. H.; Hansen, T. W.; Nilsson, A.; Stephens, I. E. L.; Chorkendorff, I., Mass-selected nanoparticles of PtxY as model catalysts for oxygen electroreduction. *Nat. Chem.* **2014,** *6* (8), 732-738.

(16) Yang, X.; Roling, L. T.; Vara, M.; Elnabawy, A. O.; Zhao, M.; Hood, Z. D.; Bao, S.; Mavrikakis, M.; Xia, Y., Synthesis and Characterization of Pt–Ag Alloy Nanocages with Enhanced Activity and Durability toward Oxygen Reduction. *Nano Lett.* **2016,** *16* (10), 6644-6649.

(17) Stephens, I. E. L.; Bondarenko, A. S.; Grønbjerg, U.; Rossmeisl, J.; Chorkendorff, I., Understanding the electrocatalysis of oxygen reduction on platinum and its alloys. *Energy Environ. Sci.* **2012,** *5* (5), 6744-6762.

(18) Briega-Martos, V.; Costa-Figueiredo, M.; Orts, J. M.; Rodes, A.; Koper, M. T. M.; Herrero, E.; Feliu, J. M., Acetonitrile Adsorption on Pt Single-Crystal Electrodes and Its Effect on Oxygen Reduction Reaction in Acidic and Alkaline Aqueous Solutions. *J. Phys. Chem. C* **2019,** *123* (4), 2300-2313.

(19) Holewinski, A.; Idrobo, J.-C.; Linic, S., High-performance Ag–Co alloy catalysts for electrochemical oxygen reduction. *Nat. Chem.* **2014,** *6* (9), 828-834.

(20) Sun, M.; Davenport, D.; Liu, H.; Qu, J.; Elimelech, M.; Li, J., Highly efficient and sustainable non-precious-metal Fe–N–C electrocatalysts for the oxygen reduction reaction. *J. Mater. Chem. A* **2018,** *6* (6), 2527-2539.

(21) Wang, M.-Q.; Yang, W.-H.; Wang, H.-H.; Chen, C.; Zhou, Z.-Y.; Sun, S.-G., Pyrolyzed Fe–N–C Composite as an Efficient Non-precious Metal Catalyst for Oxygen Reduction Reaction in Acidic Medium. *ACS Catal.* **2014,** *4* (11), 3928-3936.

(22) Tong, M.; Wang, L.; Fu, H., Designed Synthesis and Catalytic Mechanisms of

Non-Precious Metal Single-Atom Catalysts for Oxygen Reduction Reaction. *Small Methods* **2021,** *5* (10), 2100865.

(23) Kreider, M. E.; Gallo, A.; Back, S.; Liu, Y.; Siahrostami, S.; Nordlund, D.; Sinclair, R.; Nørskov, J. K.; King, L. A.; Jaramillo, T. F., Precious Metal-Free Nickel Nitride Catalyst for the Oxygen Reduction Reaction. *ACS Applied Materials & Interfaces* **2019,** *11* (30), 26863-26871.

(24) Bullock, R. M.; Chen, J. G.; Gagliardi, L.; Chirik, P. J.; Farha, O. K.; Hendon, C. H.; Jones, C. W.; Keith, J. A.; Klosin, J.; Minteer, S. D.; Morris, R. H.; Radosevich, A. T.; Rauchfuss, T. B.; Strotman, N. A.; Vojvodic, A.; Ward, T. R.; Yang, J. Y.; Surendranath, Y., Using nature's blueprint to expand catalysis with Earth-abundant metals. *Science* **2020,** *369* (6505), eabc3183.

(25) Weinberg, D. R.; Gagliardi, C. J.; Hull, J. F.; Murphy, C. F.; Kent, C. A.; Westlake, B. C.; Paul, A.; Ess, D. H.; McCafferty, D. G.; Meyer, T. J., Proton-Coupled Electron Transfer. *Chem. Rev.* **2012,** *112* (7), 4016-4093.

(26) Gómez-Marín, A.; Feliu, J.; Edson, T., Reaction Mechanism for Oxygen Reduction on Platinum: Existence of a Fast Initial Chemical Step and a Soluble Species Different from H_2O_2. *ACS Catal.* **2018,** *8* (9), 7931-7943.

(27) Ricke, N. D.; Murray, A. T.; Shepherd, J. J.; Welborn, M. G.; Fukushima, T.; Van Voorhis, T.; Surendranath, Y., Molecular-Level Insights into Oxygen Reduction Catalysis by Graphite-Conjugated Active Sites. *ACS Catal.* **2017,** *7* (11), 7680-7687.

(28) Elwell, C. E.; Gagnon, N. L.; Neisen, B. D.; Dhar, D.; Spaeth, A. D.; Yee, G. M.; Tolman, W. B., Copper-Oxygen Complexes Revisited: Structures, Spectroscopy, and Reactivity. *Chem. Rev.* **2017,** *117* (3), 2059-2107.

(29) Agarwal, R. G.; Coste, S. C.; Groff, B. D.; Heuer, A. M.; Noh, H.; Parada, G. A.; Wise, C. F.; Nichols, E. M.; Warren, J. J.; Mayer, J. M., Free Energies of Proton-Coupled Electron Transfer Reagents and Their Applications. *Chem. Rev.* **2022,** *122* (1), 1-49.

(30) Bhagi-Damodaran, A.; Michael, M. A.; Zhu, Q.; Reed, J.; Sandoval, B. A.; Mirts, E. N.; Chakraborty, S.; Moënne-Loccoz, P.; Zhang, Y.; Lu, Y., Why copper is preferred over iron for oxygen activation and reduction in haem-copper oxidases. *Nat. Chem.* **2017,** *9* (3), 257-263.

(31) Trammell, R.; Rajabimoghadam, K.; Garcia-Bosch, I., Copper-Promoted Functionalization of Organic Molecules: from Biologically Relevant Cu/O_2 Model Systems to Organometallic Transformations. *Chem. Rev.* **2019,** *119* (4), 2954-3031.

(32) Thorseth, M. A.; Tornow, C. E.; Tse, E. C. M.; Gewirth, A. A., Cu complexes that catalyze the oxygen reduction reaction. *Coord. Chem. Rev.* **2013,** *257* (1), 130-139.

(33) Chumillas, S.; Maestro, B.; Feliu, J. M.; Climent, V., Comprehensive Study of the Enzymatic Catalysis of the Electrochemical Oxygen Reduction Reaction (ORR) by Immobilized Copper Efflux Oxidase (CueO) From Escherichia coli. *Front. Chem.* **2018,** *6*.

(34) Pegis, M. L.; Martin, D. J.; Wise, C. F.; Brezny, A. C.; Johnson, S. I.; Johnson, L. E.; Kumar, N.; Raugei, S.; Mayer, J. M., Mechanism of Catalytic O_2 Reduction by Iron Tetraphenylporphyrin. *J. Am. Chem. Soc.* **2019,** *141* (20), 8315-8326.

(35) Mukherjee, M.; Dey, A., Rejigging Electron and Proton Transfer to Transition between Dioxygenase, Monooxygenase, Peroxygenase, and Oxygen Reduction Activity: Insights from Bioinspired Constructs of Heme Enzymes. *JACS Au* **2021,** *1* (9), 1296-1311.

(36) Valles, M.; Kamaruddin, A. F.; Wong, L. S.; Blanford, C. F., Inhibition in multicopper oxidases: a critical review. *Catal. Sci. Technol.* **2020,** *10* (16), 5386-5410.

(37) Macedo, L. J. A.; Hassan, A.; Sedenho, G. C.; Crespilho, F. N., Assessing electron transfer reactions and catalysis in multicopper oxidases with operando X-ray absorption spectroscopy. *Nat. Commun.* **2020,** *11* (1), 316.

(38) Wang, W.; Anderson, C. F.; Wang, Z.; Wu, W.; Cui, H.; Liu, C.-J., Peptide-templated noble metal catalysts: syntheses and applications. *Chem. Sci.* **2017,** *8* (5), 3310-3324.

(39) Yu, Y.; Cui, C.; Liu, X.; Petrik, I. D.; Wang, J.; Lu, Y., A Designed Metalloenzyme Achieving the Catalytic Rate of a Native Enzyme. *J. Am. Chem. Soc.* **2015,** *137* (36), 11570-11573.

(40) Gil-Ramírez, G.; Leigh, D. A.; Stephens, A. J., Catenanes: Fifty Years of Molecular Links. *Angew. Chem. Int. Ed.* **2015,** *54* (21), 6110-6150.

(41) Au-Yeung, H. Y.; Deng, Y., Distinctive features and challenges in catenane chemistry. *Chem. Sci.* **2022,** *13* (12), 3315-3334.

(42) Zhu, L.; Li, J.; Yang, J.; Au-Yeung, H. Y., Cross dehydrogenative C–O coupling catalysed by a catenane-coordinated copper(I). *Chem. Sci.* **2020,** *11* (48), 13008-13014.

(43) Jiao, Y.; Đorđević, L.; Mao, H.; Young, R. M.; Jaynes, T.; Chen, H.; Qiu, Y.; Cai, K.; Zhang, L.; Chen, X.-Y.; Feng, Y.; Wasielewski, M. R.; Stupp, S. I.; Stoddart, J. F., A Donor–Acceptor [2]Catenane for Visible Light Photocatalysis. *J. Am. Chem. Soc.* **2021,** *143* (21), 8000-8010.

(44) Mitra, R.; Zhu, H.; Grimme, S.; Niemeyer, J., Functional Mechanically Interlocked Molecules: Asymmetric Organocatalysis with a Catenated Bifunctional Brønsted Acid. *Angew. Chem. Int. Ed.* **2017,** *56* (38), 11456-11459.

(45) Leigh, D. A.; Marcos, V.; Wilson, M. R., Rotaxane Catalysts. *ACS Catal.* **2014,** *4* (12), 4490-4497.

(46) Kwamen, C.; Niemeyer, J., Functional Rotaxanes in Catalysis. *Chem. Eur. J.* **2021,** *27* (1), 175-186.

(47) Martinez-Cuezva, A.; Saura-Sanmartin, A.; Alajarin, M.; Berna, J., Mechanically Interlocked Catalysts for Asymmetric Synthesis. *ACS Catal.* **2020,** *10* (14), 7719-7733.

(48) Heard, A. W.; Suárez, J. M.; Goldup, S. M., Controlling catalyst activity, chemoselectivity and stereoselectivity with the mechanical bond. *Nat. Rev. Chem.* **2022,** *6* (3), 182-196.

(49) Yee, C.-C.; Ng, A. W. H.; Au-Yeung, H. Y., Control over the macrocyclisation pathway and product topology in a copper-templated catenane synthesis. *Chem. Commun.* **2019,** *55* (44), 6169-6172.

(50) Dietrich-Buchecker, C. O.; Sauvage, J. P.; Kintzinger, J. P., Une nouvelle famille de molecules : les metallo-catenanes. *Tetrahedron Lett.* **1983,** *24* (46),

5095-5098.
(51) Dietrich-Buchecker, C. O.; Sauvage, J. P.; Kern, J. M., Templated synthesis of interlocked macrocyclic ligands: the catenands. *J. Am. Chem. Soc.* **1984,** *106* (10), 3043-3045.
(52) Dietrich-Buchecker, C.; Sauvage, J. P.; Kern, J. M., Synthesis and electrochemical studies of catenates: stabilization of low oxidation states by interlocked macrocyclic ligands. *J. Am. Chem. Soc.* **1989,** *111* (20), 7791-7800.
(53) Albrecht-Gary, A. M.; Saad, Z.; Dietrich-Buchecker, C. O.; Sauvage, J. P., Interlocked macrocyclic ligands: a kinetic catenand effect in copper(I) complexes. *J. Am. Chem. Soc.* **1985,** *107* (11), 3205-3209.
(54) Cirulli, M.; Kaur, A.; Lewis, J. E. M.; Zhang, Z.; Kitchen, J. A.; Goldup, S. M.; Roessler, M. M., Rotaxane-Based Transition Metal Complexes: Effect of the Mechanical Bond on Structure and Electronic Properties. *J. Am. Chem. Soc.* **2019,** *141* (2), 879-889.
(55) McCrory, C. C. L.; Ottenwaelder, X.; Stack, T. D. P.; Chidsey, C. E. D., Kinetic and Mechanistic Studies of the Electrocatalytic Reduction of O_2 to H_2O with Mononuclear Cu Complexes of Substituted 1,10-Phenanthrolines. *J. Phys. Chem. A* **2007,** *111* (49), 12641-12650.
(56) McCrory, C. C. L.; Devadoss, A.; Ottenwaelder, X.; Lowe, R. D.; Stack, T. D. P.; Chidsey, C. E. D., Electrocatalytic O_2 Reduction by Covalently Immobilized Mononuclear Copper(I) Complexes: Evidence for a Binuclear Cu_2O_2 Intermediate. *J. Am. Chem. Soc.* **2011,** *133* (11), 3696-3699.
(57) Thorseth, M. A.; Letko, C. S.; Tse, E. C. M.; Rauchfuss, T. B.; Gewirth, A. A., Ligand Effects on the Overpotential for Dioxygen Reduction by Tris(2-pyridylmethyl)amine Derivatives. *Inorg. Chem.* **2013,** *52* (2), 628-634.
(58) Tse, E. C. M.; Schilter, D.; Gray, D. L.; Rauchfuss, T. B.; Gewirth, A. A., Multicopper Models for the Laccase Active Site: Effect of Nuclearity on Electrocatalytic Oxygen Reduction. *Inorg. Chem.* **2014,** *53* (16), 8505-8516.
(59) Glowacki, D. R.; Harvey, J. N.; Mulholland, A. J., Taking Ockham's razor to enzyme dynamics and catalysis. *Nat. Chem.* **2012,** *4* (3), 169-176.
(60) Zhang, J.; Balsbaugh, J. L.; Gao, S.; Ahn, N. G.; Klinman, J. P., Hydrogen deuterium exchange defines catalytically linked regions of protein flexibility in the catechol *O*-methyltransferase reaction. *Proc. Natl. Acad. Sci. USA* **2020,** *117* (20), 10797-10805.
(61) Luk, L. Y. P.; Ruiz-Pernía, J. J.; Dawson, W. M.; Roca, M.; Loveridge, E. J.; Glowacki, D. R.; Harvey, J. N.; Mulholland, A. J.; Tuñón, I.; Moliner, V.; Allemann, R. K., Unraveling the role of protein dynamics in dihydrofolate reductase catalysis. *Proc. Natl. Acad. Sci. USA* **2013,** *110* (41), 16344-16349.
(62) Mo, X.; Chan, K. C.; Tse, E. C. M., A Scalable Laser-Assisted Method to Produce Active and Robust Graphene-Supported Nanoparticle Electrocatalysts. *Chem. Mater.* **2019,** *31* (19), 8230-8238.
(63) Tse, E. C. M.; Barile, C. J.; Kirchschlager, N. A.; Li, Y.; Gewargis, J. P.; Zimmerman, S. C.; Hosseini, A.; Gewirth, A. A., Proton transfer dynamics control the mechanism of O_2 reduction by a non-precious metal electrocatalyst. *Nat. Mater.* **2016,**

15 (7), 754-759.

(64) Varnell, J. A.; Tse, E. C. M.; Schulz, C. E.; Fister, T. T.; Haasch, R. T.; Timoshenko, J.; Frenkel, A. I.; Gewirth, A. A., Identification of carbon-encapsulated iron nanoparticles as active species in non-precious metal oxygen reduction catalysts. *Nat. Commun.* **2016,** *7* (1), 12582.

(65) Zeng, T.; Gautam, R. P.; Barile, C. J.; Li, Y.; Tse, E. C. M., Nitrile-Facilitated Proton Transfer for Enhanced Oxygen Reduction by Hybrid Electrocatalysts. *ACS Catal.* **2020,** *10* (21), 13149-13155.

(66) Wang, W.; Tse, E. C. M., Proton Removal Kinetics That Govern the Hydrogen Peroxide Oxidation Activity of Heterogeneous Bioinorganic Platforms. *Inorg. Chem.* **2021,** *60* (10), 6900-6910.

(67) Paulus, U. A.; Schmidt, T. J.; Gasteiger, H. A.; Behm, R. J., Oxygen reduction on a high-surface area Pt/Vulcan carbon catalyst: a thin-film rotating ring-disk electrode study. *J. Electroanal. Chem.* **2001,** *495* (2), 134-145.

(68) Naresh Kumar, T.; Sivabalan, S.; Chandrasekaran, N.; Phani, K. L., Synergism between polyurethane and polydopamine in the synthesis of Ni–Fe alloy monoliths. *Chem. Commun.* **2015,** *51* (10), 1922-1925.

(69) Ravel, B.; Newville, M., ATHENA, ARTEMIS, HEPHAESTUS: data analysis for X-ray absorption spectroscopy using IFEFFIT. *J Synchrotron Radiat.* **2005,** *12* (Pt 4), 537-41.

(70) Frisch, M.; Trucks, G.; Schlegel, H.; Scuseria, G.; Robb, M.; Cheeseman, J.; Scalmani, G.; Barone, V.; Mennucci, B.; Petersson, G., GAUSSIAN09. Gaussian Inc., Wallingford, CT, USA. 2009.

(71) Hanwell, M. D.; Curtis, D. E.; Lonie, D. C.; Vandermeersch, T.; Zurek, E.; Hutchison, G. R., Avogadro: an advanced semantic chemical editor, visualization, and analysis platform. *J. Cheminform.* **2012,** *4* (1), 17.

(72) Becke, A. D., Density-functional thermochemistry. III. The role of exact exchange. *Chem. Phys.* **1993,** *98* (7), 5648-5652.

(73) Lee, C.; Yang, W.; Parr, R. G., Development of the Colle-Salvetti correlation-energy formula into a functional of the electron density. *Phys. Rev. B* **1988,** *37* (2), 785-789.

(74) Stephens, P. J.; Devlin, F. J.; Chabalowski, C. F.; Frisch, M. J., Ab Initio Calculation of Vibrational Absorption and Circular Dichroism Spectra Using Density Functional Force Fields. *J. Phys. Chem. A* **1994,** *98* (45), 11623-11627.

(75) Cowley, R. E.; Tian, L.; Solomon, E. I., Mechanism of O_2 activation and substrate hydroxylation in noncoupled binuclear copper monooxygenases. *Proc. Natl. Acad. Sci. USA* **2016,** *113* (43), 12035-12040.

(76) Ben El Ayouchia, H.; Bahsis, L.; Anane, H.; Domingo, L. R.; Stiriba, S.-E., Understanding the mechanism and regioselectivity of the copper(I) catalyzed [3 + 2] cycloaddition reaction between azide and alkyne: a systematic DFT study. *RSC Adv.* **2018,** *8* (14), 7670-7678.

(77) Yang, Y.; Weaver, M. N.; Merz, K. M., Assessment of the "6-31+G** + LANL2DZ" Mixed Basis Set Coupled with Density Functional Theory Methods and the Effective Core Potential: Prediction of Heats of Formation and Ionization

Potentials for First-Row-Transition-Metal Complexes. *J. Phys. Chem. A* **2009,** *113* (36), 9843-9851.
(78) Hay, P. J.; Wadt, W. R., Ab initio effective core potentials for molecular calculations. Potentials for the transition metal atoms Sc to Hg. *J. Chem. Phys* **1985,** *82* (1), 270-283.
(79) Wadt, W. R.; Hay, P. J., Ab initio effective core potentials for molecular calculations. Potentials for main group elements Na to Bi. *J. Chem. Phys* **1985,** *82* (1), 284-298.
(80) Tomasi, J.; Mennucci, B.; Cammi, R., Quantum Mechanical Continuum Solvation Models. *Chem. Rev.* **2005,** *105* (8), 2999-3094.
(81) Pettersen, E. F.; Goddard, T. D.; Huang, C. C.; Couch, G. S.; Greenblatt, D. M.; Meng, E. C.; Ferrin, T. E., UCSF Chimera—A visualization system for exploratory research and analysis. *J. Comput. Chem.* **2004,** *25* (13), 1605-1612.

Acknowledgements

E.C.M.T. would like to express our gratitude to the Hong Kong (HK) Research Grants Council (RGC) for supporting our research program via an Early Career Scheme (RGC: 27301120). H.Y.A.Y. acknowledges the support from the CAS-Croucher Funding Scheme for Joint Laboratories. The authors would like to thank the CAS-RGC Joint Laboratory Funding Scheme (RGC: JLFS/P-704/18) for upgrading the materials characterization infrastructure at the HKU-CAS Joint Laboratory on New Materials. X.M. would like to thank the Algaia Outstanding RPg Student Award. Y.D. would like to thank Jo Yip and Bonnie Yan at the Department of Chemistry at HKU for their help with mass spectrometry and NMR measurements. S.K.M.L. and X.G. would like to recognize the High-Performance Computing (HPC) services offered by ITS at HKU for mechanistic investigations. H.L.W. thanks financial support by the Center of Atomic Initiative for New Materials, National Taiwan University, from the Featured Areas Research Center Program within the framework of the Higher Education Sprout Project by the Ministry of Education in Taiwan (108L9008), and MOST (Ministry of Science and Technology), Taiwan (Contracts No. 110-2113-M-002 -019 -MY3).

Author information

These authors contributed equally: Xiaoyong Mo, Yulin Deng

Affiliations

Department of Chemistry, HKU-CAS Joint Laboratory of New Materials, University of Hong Kong, Hong Kong SAR, China

Xiaoyong Mo, Yulin Deng, Samuel Kin-Man Lai, Xutao Gao, Kam-Hung Low, Ho Yu Au-Yeung & Edmund C. M. Tse

HKU Zhejiang Institute of Research and Innovation, Zhejiang 311305, China

Edmund C. M. Tse

Center for Condensed Matter Sciences, National Taiwan University, Taipei, 10617, Taiwan

Hung-Ling Yu & Heng-Liang Wu

Center of Atomic Initiative for New Materials, National Taiwan University, Taipei, 10617, Taiwan

Hung-Ling Yu & Heng-Liang Wu

State Key Laboratory of Synthetic Chemistry, University of Hong Kong, Hong Kong SAR, China

Ho Yu Au-Yeung

Author contributions

X.M. and Y.D. contributed equally to this work. A.Y.H.Y. and E.C.M.T. conceived the idea for this work. X.M. and Y.D. designed the research strategy. Y.D. performed molecular synthesis and characterization, while X.M. assessed the electrocatalytic performance of the compounds and carried out mechanistic studies. K.H.L. was responsible for single-crystal X-ray diffraction measurement and X-ray structural determination. H.L.Y. acquired and analysed XAS data with help from H.L.W. S.K.M.L. performed DFT calculations aided by X.G. A.Y.H.Y. and E.C.M.T. supervised the project. A.Y.H.Y. and E.C.M.T. wrote the manuscript with contributions from all authors.

Corresponding Authors. HYAY: hoyuay@hku.hk; ECMT: ecmtse@hku.hk

Competing interests

The authors declare no competing financial interests.

Additional information

Supporting information The online version contains supplementary material (including experimental details, synthetic procedures, NMR and MS characterization data, single crystal X-ray crystallography results, control experiments, kinetic isotope effect studies, anion effect studies, Tafel slope analyses, synchrotron XAS data, ICP-MS results, cyclic voltammograms, linear sweep voltammograms, theoretical calculations, computational modelling results, simulated structures, supplementary tables, additional notes, and supporting figures) available at

Correspondence and requests for materials should be addressed to Ho Yu Au-Yeung and Edmund C. M. Tse.

Graphical abstract

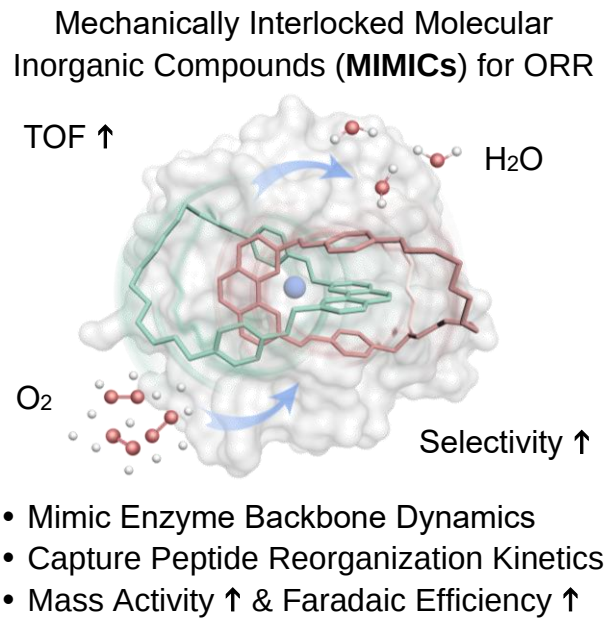

Synopsis

Mechanically interlocked molecular inorganic compounds (MIMICs) enhance O_2 reduction reaction (ORR) turnover frequency (TOF), mass activity, selectivity for $4e^-$ pathway, and Faradaic efficiency for H_2O by capturing the structural dynamics of metalloenzyme polypeptide backbones through optimizing the rearrangement kinetics of mechanical bonds.